High-Yield Dispersions of Large-Diameter Semiconducting Single-Walled Carbon Nanotubes with Tunable Narrow Chirality Distributions

Kevin S. Mistry,[†,‡] Brian A. Larsen,[†] and Jeffrey L. Blackburn[†,*]

[†]National Renewable Energy Laboratory, Golden, Colorado 80401, United States and [‡]Department of Physics, University of Colorado, Boulder, Colorado 80309, United States

ABSTRACT Here, we report a thorough study on the ability of fluorene-based semiconducting polymers to disperse large-diameter (average diameter $\langle d \rangle \approx 1.3$ nm) laser vaporization (LV) single-walled carbon nanotubes (SWCNTs). We demonstrate the ability to select purely semiconducting species using poly[(9,9-dioctylfluorenyl-2,7-diyl)-*alt*-*co*-(6,6′-{2,2′-bipyridine})] (PFO-BPy) and poly[(9,9-dihexylfluorenyl-2,7-diyl)-*co*-(9,10-anthracene)] (PFH-A), producing samples with narrow and bright excitonic emission relative to comparable aqueous dispersions. Rapid processing and high yields offer the ability to easily incorporate these semiconducting SWCNTs into commercially scalable applications, as demonstrated by large-area thin films prepared by ultrasonic spraying. By modifying the growth temperature of the LV synthesis, we demonstrate the ability to tune the range of diameters and chiralities within dispersions by exerting synthetic control over the composition of the starting material. This synthetic control allows us to show that PFH-A preferentially disperses near-armchair semiconducting SWCNTs over a large range of diameters (0.8 nm < d < 1.4 nm) and induces unique solvatochromic shifts for the excitonic transitions of nanotubes with particular chiral indices.

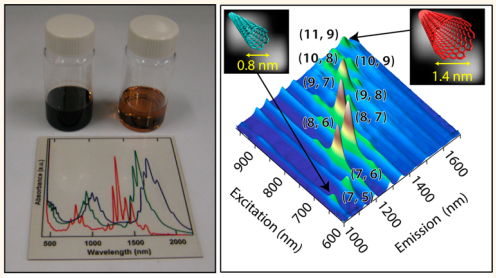

High Purity and Concentration | Chiral Angle Selectivity

KEYWORDS: carbon nanotube · photovoltaic · separations · enrichment · semiconducting · SWCNT · FET · field-effect transistor · polymer

All current synthesis methods for SWCNTs produce both metallic (m-) and semiconducting (s-) species, typically with ~33% metallic content, but as low as ~8% for the small-diameter ($d \approx$ 0.8 nm) CoMoCat process.[1] A number of applications envisioned for SWCNTs, such as photovoltaic (PV) active layers,[2−4] field-effect transistors (FETs),[5−7] and logic circuits,[8] specifically require s-SWCNTs with minimal m-SWCNT impurities. To further enrich samples in semiconducting species, researchers have developed several postsynthetic strategies, including density gradient ultracentrifugation (DGU),[9] column chromatography,[10] and selective dispersion using aromatic polymers.[11] DGU and column chromatography have been applied to a wide range of SWCNT diameters, but tend to suffer from low throughput for reaching purities and yields necessary for large-scale production of devices. Selective dispersion using polymers, polyfluorene derivatives in particular, has emerged as a powerful and scalable strategy for enriching small-diameter s-SWCNTs,[11−13] but has been minimally explored for larger diameter (d > 1.2 nm) SWCNTs.[14,15]

Scalable purification and enrichment processes are required for a number of applications that may benefit specifically from larger diameter s-SWCNTs. For example, thin-film SWCNT FETs[9,16] require metallic content less than ~2%, while the ultimate goal for digital logic[8] is in the range of parts-per-million to parts-per-billion m-SWCNT impurities. FET performance is enhanced by using nanotubes with d > 1.2 nm, which reduce current-limiting Schottky barriers and dramatically improve the on/off ratio relative to small-diameter SWCNTs.[5]

* Address correspondence to jeffrey.blackburn@nrel.gov.

Received for review November 16, 2012 and accepted February 4, 2013.

Published online February 04, 2013
10.1021/nn305336x

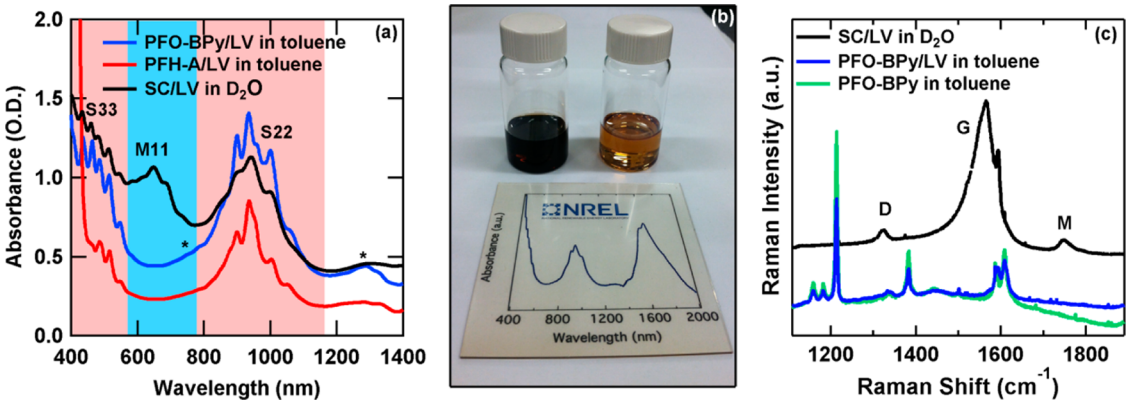

Figure 1. (a) Absorbance spectra of LV SWCNTs dispersed by SC, PFO-BPy, and PFH-A. Spectra were taken in a 5 mm path length cuvette for the polymer dispersions in toluene and a 2 mm path length cuvette for SC/LV. Asterisks mark the positions of vibronic optical transitions for the s-SWCNTs. (b) Photograph of a PFO-BPy dispersion (top left) and a dilute PFH-A dispersion (top right) along with a film of PFO-BPy-wrapped SWCNTs deposited by ultrasonic spraying onto a 3 in. × 3 in. glass substrate. The absorbance spectrum for the film is shown underneath the film. Full absorbance spectra (400−2200 nm) for the PFO-BPY and PFH-A dispersions and films shown in (a) and (b) are given in the Supporting Information (Figure S3). (c) Raman spectra of SC/LV in D_2O, PFO-BPy/LV in toluene, and PFO-BPy in toluene. Signatures of m-SWCNTs are clearly visible in the SC/LV sample and absent in the other two. Spectra have been offset for visibility. LV synthesis temperature for all three panels was 1125 °C.

Increased carrier mobility, which scales quadratically with nanotube diameter,[17] may also improve FETs and PV devices that incorporate large-diameter SWCNTs. In PV devices, large-diameter s-SWCNTs cover a larger range of the solar spectrum by absorbing deeper into the infrared (IR) and may also form type II heterojunctions with low band gap polymers[18] or high electron affinity fullerenes,[19] potentially increasing efficiencies of SWCNT PV active layers. SWCNT PV active layers based on large-diameter SWCNTs may also realize enhanced efficiencies by exploiting multiple exciton generation (MEG) in the visible and near-IR, as opposed to small-diameter SWCNTs, which exhibit MEG primarily in the ultraviolet region.[20] Lastly, enriched s-SWCNTs that absorb around 1530−1565 nm (1.3 nm < d < 1.4 nm) would be useful as photonic elements in telecommunications applications.[21]

In this study, we examine the ability of nine separate fluorene-based semiconducting polymers to selectively wrap large-diameter SWCNTs produced by laser vaporization (LV). Two polymers in particular, poly[(9,9-dioctylfluorenyl-2,7-diyl)-*alt*-*co*-(6,6′-{2,2′-bipyridine})] (PFO-BPy) and poly[(9,9-dihexylfluorenyl-2,7-diyl)-*co*-(9,10-anthracene)] (PFH-A), demonstrate the ability to exclusively select large-diameter semiconducting species with high yields critical to scalable device fabrication and higher luminescence intensities than typical aqueous dispersions. While PFO-BPy shows no selectivity for particular large-diameter s-SWCNTs, PFH-A disperses narrow chirality distributions composed primarily of near-armchair s-SWCNTs and interacts uniquely with particular chiral indices. The results obtained here enable a better fundamental understanding of how aromatic polymers select particular SWCNTs to produce the highly enriched samples needed to move toward commercial applications requiring semiconducting SWCNTs. Additionally, the high-yield/high-purity s-SWCNT samples demonstrated here can be easily integrated into high-efficiency field-effect transistors and solar cells and should immediately impact the fields of SWCNT digital logic and photovoltaics.

RESULTS AND DISCUSSION

We first tested the ability of fluorene-based polymers to disperse LV SWCNTs produced at our typical synthesis temperature of 1125 °C ($\langle d \rangle \approx 1.3$ nm). Figure 1a demonstrates that two polymers in particular, both PFO-BPy and PFH-A, disperse high concentrations of these large-diameter SWCNTs with undetectable contributions from metallic SWCNTs. The optical density (OD) for the PFO-BPy-wrapped LV SWCNTs in a 5 mm path length cuvette is greater than 1.0 for most of the third (S_{33}) and second (S_{22}) semiconducting exciton peaks. With a peak S_{22} OD > 1.4 at 935 nm, these concentrations are significantly higher than any other reports using fluorene-based polymers on large-diameter arc-discharge[15] (S_{22} OD ≈ 0.01) or LV SWCNTs[23] (S_{22} OD < 0.2 in 10 mm cuvette). Furthermore, these results can be produced rapidly (<1 h), in contrast to methods such as DGU that typically require steps of 18−24 h, produce relatively small quantities, and often require multiple iterations to produce high s-SWCNT enrichment (*e.g.*, >99%).[9,24] Interestingly, Berton *et al.* recently reported on a fluorene-based polymer with anthracene subunits (similar to PFH-A) that dispersed large-diameter LV SWCNTs, but required an additional DGU step to remove m-SWCNTs that lowered the yield (S_{22} OD ≈ 0.1).[14] Using thermogravimetric analysis (TGA) and absorbance spectroscopy (detailed description in the Supporting Information, Figures S1 and S2), we found that, for the sample shown in Figure 1a, PFO-BPy dispersed ∼1/3 of the s-SWCNTs present in the raw SWCNT material *without any other purification or centrifugation steps required prior to dispersion*. Since device cost is intimately tied to raw

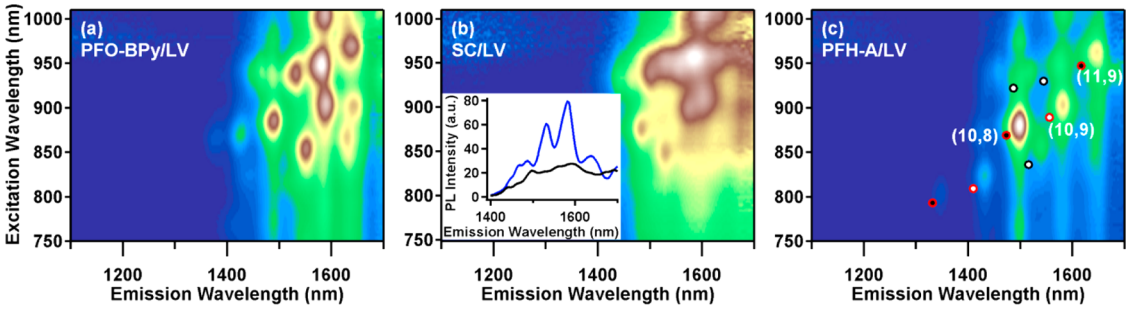

Figure 2. PLE maps of (a) PFO-BPy/LV, (b) SC/LV, and (c) PFH-A/LV. The inset shows a PL slice of PFO-BPy/LV (blue) and SC/LV (black) at 935 nm when both solutions had the same optical density. The PL intensity for the PFO-BPy/LV solution is ~3 times higher than the SC/LV solution. Circles indicate positions of s-SWCNT chiralities as reported by Weisman *et al.*[32] Circles in red are near-armchair chiralities, with $q = \mathrm{mod}(n - m, 3) = 2$ species filled in black. LV synthesis temperature for all three panels was 1125 °C. Full chirality assignments are omitted in (a) and (b) to avoid congestion, but are given in the Supporting Information (Figures S12−S14).

material yield, our high-yield dispersions lend themselves naturally to commercial-scale production that will be necessary for future electronics applications. As demonstrated in Figure 1b, the highly concentrated SWCNT inks enabled by these polymers are easily integrated into roll-to-roll solution deposition strategies (*e.g.*, ultrasonic spraying)[22] for thin-film transistors or PV materials. The 3 × 3 in. film shown in Figure 1b required only a few milliliters of solution to fabricate and was sprayed in minutes.

In addition to commercially relevant yields, both absorbance and Raman spectroscopy demonstrate undetectable m-SWCNT impurities. The first metallic excitonic transitions (M_{11}), visible in Figure 1a for (nonselective) sodium cholate (SC)-dispersed LV SWCNTs, are completely absent for the same SWCNTs dispersed with PFO-BPy and PFH-A. In Figure 1a, asterisks mark the positions of vibronic optical transitions for the s-SWCNTs, arising from coupling of A_1' phonons to momentum-forbidden dark excitons.[25] These peaks also appear in the excitation scans extracted from PLE maps (Supporting Information, Figures S4 and S5). It is important to differentiate the s-SWCNT vibronic peaks from optical transitions of m-SWCNTs since they appear in a range (~700−800 nm) similar to that expected for the excitonic transitions of the largest diameter m-SWCNTs within this diameter distribution. For a more detailed discussion, we refer the reader to the Supporting Information. To further verify the selectivity of these polymers, we looked for signatures of m-SWCNTs using Raman spectroscopy with a probe wavelength of 632.8 nm (1.96 eV), resonant with the M_{11} transitions of our LV m-SWCNTs ($\langle d \rangle \approx 1.3$ nm). In our control sample of SC-dispersed SWCNTs (Figure 1c), we observe clear signatures assigned to the D, G, and M bands of m-SWCNTs.[26] In contrast, for the PFO-BPy and PFH-A (Supporting Information, Figures S6 and S7) wrapped LV samples, we observe only peaks that match those from a polymer/toluene control sample (all peaks assignable to toluene), but no signs of m-SWCNT peaks.[27]

Other methods such as DGU can enrich large-diameter s-SWCNTs to 99%,[24,28] while gel electrophoresis and column chromatography typically reach up to 95%.[29,30] While not a quantitative comparison, we note that typically published absorbance spectra for large-diameter s-SWCNT samples produced by these methods have some small, but visible contributions to the absorbance spectra from m-SWCNTs. In contrast, for our PFO-BPy and PFH-A SWCNTs, we find no evidence of m-SWCNTs in the absorbance spectra or the more sensitive Raman measurements. From an analysis of the absorbance spectrum[31] and a comparison to a commercially available s-SWCNT material (Supporting Information, Figure S8), we estimate the s-SWCNT purity at >99.0%.

To determine the chiralities wrapped by each polymer, we obtained photoluminescence excitation (PLE) maps, shown in Figure 2. Most semiconducting species with S_{11} from 1400 to 1750 nm and S_{22} from 820 to 1010 nm are present in the PFO-BPy/LV PLE map.[32] A similar chirality distribution is found in the PLE map of SC-dispersed SWCNTs in D_2O (Figure 2b), suggesting that PFO-BPy does not select particular chiral indices. When compared with the same LV SWCNTs dispersed in SC (Figure 2b inset), the PFO-BPy/LV peaks are significantly narrower and the PL intensity is a factor of ~3 higher for a sample with similar OD. Increased PL intensity is consistent with recent reports that solvents with lower dielectric constants lead to higher PL quantum yields due to the reduction of excitonic screening and charge-transfer-induced exciton dissociation sites.[33,34] Water-filled SWCNTs have also been shown to produce broader peaks with lower PL quantum yield.[35] The sharper and brighter peaks of the PFO-BPy/LV sample in toluene demonstrate that large-diameter LV SWCNTs can be bright near-IR fluorophores when dispersed in low dielectric media. Additionally, these samples should facilitate future quantitative PL studies of larger diameter SWCNTs that have not previously been dispersed by organic polymers.

The absorbance spectrum of PFH-A clearly contains a reduced number of peaks in the S_{11}, S_{22}, and S_{33} regions, indicating that it selects specific chiral species of s-SWCNTs. Accordingly, the PLE map for PFH-A (Figure 2c) is dominated by near-armchair SWCNTs,

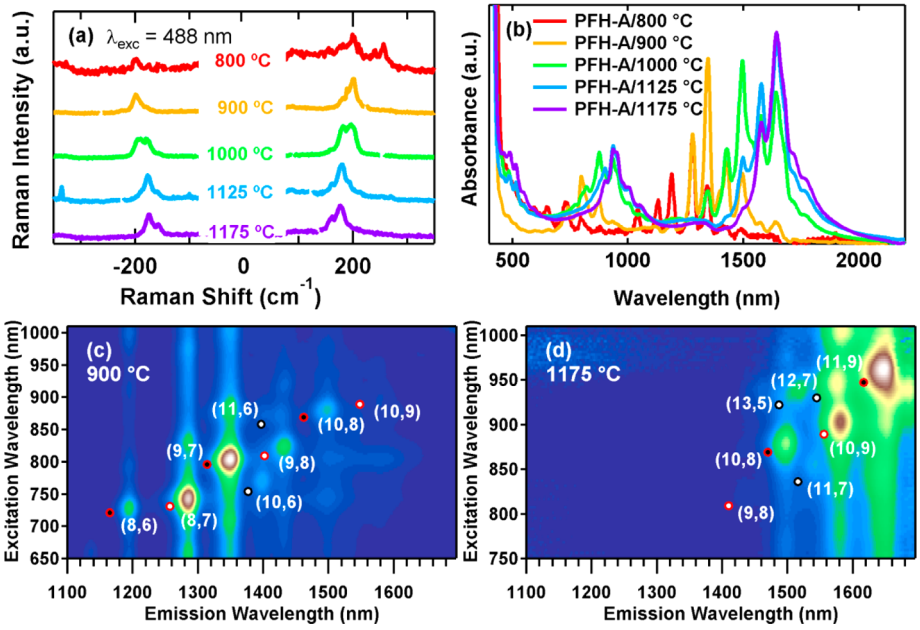

Figure 3. (a) Raman spectra of LV SWCNTs synthesized at different furnace temperatures, highlighting the region of the diameter-dependent radial breathing modes (RBM). All spectra were taken of raw SWCNT powders with an excitation wavelength of 488 nm and a power of 7 mW. (b) Normalized absorbance spectra of PFH-A-dispersed LV SWCNTs synthesized at different furnace temperatures. (c, d) PLE maps of PFH-A/LV using SWCNTs synthesized at 900 and 1175 °C, respectively.

in particular the (10,8) SWCNT (d = 1.24 nm), demonstrating the ability of this polymer to disperse narrow chirality distributions of large-diameter SWCNTs. In an attempt to probe the scope of PFH-A selectivity, we systematically manipulated the diameter distribution of the LV SWCNTs by tuning the temperature of LV synthesis away from our standard 1125 °C.[36] Figure 3a displays the radial breathing modes (RBM) of the raw SWCNTs produced by LV at different synthesis temperatures and demonstrates a systematic progression to smaller average diameter (larger RBM ω) as the furnace temperature decreases, in agreement with absorbance spectra (Figure 3b, S10 and S11). The PLE maps shown in Figure 3c and d (and others in Supporting Information, Figures S12−S14) demonstrate that PFH-A primarily selects near-armchair SWCNTs regardless of diameter. For example, samples synthesized at 1175 °C (Figure 3d) are enriched primarily in the (11,9) SWCNT, while 900 °C synthesis (Figure 3c) leads to enrichment primarily in (9,7). Figure 4a summarizes the semiconducting species dispersed by PFH-A at all synthesis temperatures, demonstrating a universal preference of PFH-A for near-armchair SWCNTs over a large-diameter range of ~0.8−1.4 nm. As the diameter increases, a small amount of SWCNTs with smaller chiral angles is observed in the PLE spectra, but these minority species represent only a small fraction of the population. These results demonstrate that the exertion of synthetic control over SWCNT diameter distribution, coupled with careful selection of wrapping polymer, can be used to rationally tune narrow chirality distributions for applications.

To better understand the underlying mechanism driving the selectivity of PFH-A for near-armchair SWCNTs, we compared the excitation (S_{22}) and emission (S_{11}) peak positions for the PFH-A and PFO-BPy dispersions. SWCNT exciton transition energies are known to be sensitive to the surrounding environment and undergo what are generally referred to as solvatochromic shifts when the surrounding dielectric medium is changed significantly.[33] Thus, we expected to observe different trends for the S_{11} and S_{22} solvatochromic shifts of PFH-A-dispersed near-armchair SWCNTs when compared to minority species with smaller chiral angles. Figure 4b displays the shifts in S_{11} and S_{22} exciton energies (ΔS_{11} and ΔS_{22}) of SWCNTs dispersed with PFH-A relative to the energies observed in PFO-BPy. We chose the PFO-BPy exciton energies for normalization since PFO-BPy does not exhibit any chiral selectivity for large-diameter SWCNTs. Surprisingly, we found significant differences in shifts only for the near-armchair SWCNTs in the q = mod($n - m$, 3) = 2 family, as compared to all other SWCNTs dispersed with PFH-A (Supporting Information, Table S1). As shown in Figure 4b, the S_{22} energies for the (7,5), (8,6), (9,7), (10,8), and (11,9) SWCNTs exhibit large blue-shifts (~ 4−9 meV) in the PFH-A sample (relative to PFO-BPy). In contrast, all other chiralities, *including q = 1 near-armchair SWCNTs*, display either no shift or very small shifts, with most of these species exhibiting red-shifts. Additionally, the S_{11} energies for these five SWCNTs have red-shifts of 3.7−8.0 meV in the PFH-A sample compared to PFO-BPy (inversely correlated with diameter), while all other chiralities display a blue-shift. These marked differences suggest a change in the local dielectric environment around PFH-A-dispersed q = 2 near-armchair nanotubes[33] that is not experienced by

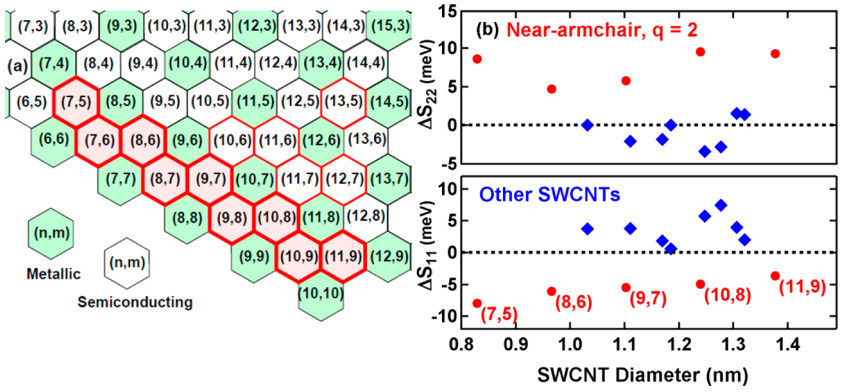

Figure 4. (a) Section of the graphene sheet near the arm-chair edge ($\theta = 30°$). Semiconducting LV SWCNTs dispersed by PFH-A are denoted by red hexagons. Thick hexagons represent majority species, while thin hexagons represent minority species. (b) Shifts of S_{11} and S_{22} peak positions in PFH-A dispersions relative to PFO-BPy. Near-armchair $q = 2$ SWCNTs (red circles) reveal distinct trends, while other chiralities (blue diamonds) do not.

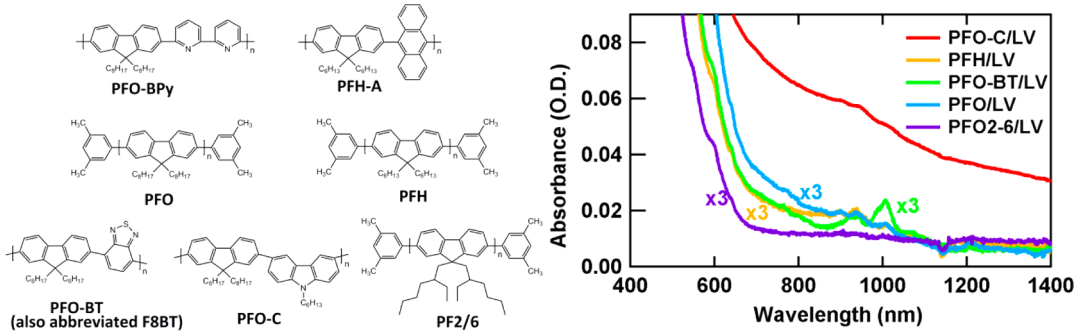

Figure 5. (a) Structures of the polymers used in this study. Full names are given in the text. We also studied the terpyridine and monopyridine analogues of PFO-BPy (Supporting Information, Figure S16). (b) Absorbance spectra for five other polyfluorene polymer/LV dispersions. LV synthesis temperature was 1125 °C. Spectra were taken in a 5 mm cuvette.

other SWCNTs dispersed by this polymer. This remarkable difference suggests that PFH-A may have different adsorption geometries based on chirality, similar to what has been predicted by molecular dynamics modeling for poly[9,9-dioctylfluorenyl-2,7-diyl] (PFO).[37] These molecular dynamics models suggest that the selectivity of PFO is driven by a combination of SWCNT diameter and chiral angle that enables helical wrapping of the polymer around the nanotube. Another recent study suggests that in some cases selectivity may be driven by the electronic overlap between polymer and SWCNT energy levels.[15] Importantly, in the current study we dramatically vary both the diameter and the diameter-dependent potentials of SWCNT orbital energy levels, so the unique shifts observed for $q = 2$ near-armchair SWCNTs cannot be explained by these mechanisms.[15,37] Instead, we suggest that the adsorption geometry of PFH-A may be sensitive to subtle changes in chiral angle, given that the $q = 2$ near-armchair SWCNTs fall within a narrow chiral angle range ($24.5° < \theta < 26.7°$). While these intriguing results do not allow us to speculate on the particular geometries adopted by PFH-A, they encourage the future use of molecular dynamics modeling to observe the potentially unique adsorption of PFH-A on near-armchair $q = 2$ SWCNTs.

Besides PFO-BPy and PFH-A, we tested several other fluorene-based polymers with our standard LV synthesis ($T = 1125$ °C) SWCNTs: PFO, poly[9,9-dihexylfluorenyl-2,7-diyl] (PFH), poly[9,9-di(2-ethylhexyl)fluorenyl-2,7-diyl] (PF2/6), poly[(9,9-dioctylfluorenyl-2,7-diyl)-*alt*-*co*-(9-hexyl-3,6-carbazole)] (PFO-C), and poly[(9,9-dioctylfluorenyl-2,7-diyl)-*alt*-*co*-(1,4-benzo-{2,1′,3}-thiadiazole)] (PFO-BT or F8BT). These five polymers showed minute or no extraction of large-diameter SWCNTs (Figure 5). We note, however, that the absorbance spectrum for PFO-BT-wrapped LV SWCNTs is similar to that reported by Tange *et al.*, who found enrichment in the (15,4) chirality.[15] The very low SWCNT concentrations dispersed by PFO-BT make it difficult to assess the presence or absence of m-SWCNTs *via* absorbance and Raman and also suggest this polymer is less useful for commercial SWCNT device applications.

Homopolymers of fluorene monomers with various alkyl chains (PFO, PFH, and PF2/6) did not exhibit any significant ability to disperse large-diameter SWCNTs. As has been observed for HiPco and CoMoCat SWCNTs, PFO was successful in dispersing smaller diameter LV SWCNTs synthesized at lower temperatures (Supporting Information, Figure S15), with dispersion ability rapidly falling off at a SWCNT diameter of ~1.1 nm (*i.e.*, (9,7) SWCNT). It is likely that this inability for the homopolymers to effectively disperse large-diameter SWCNTs is primarily a structural effect related to the steric packing

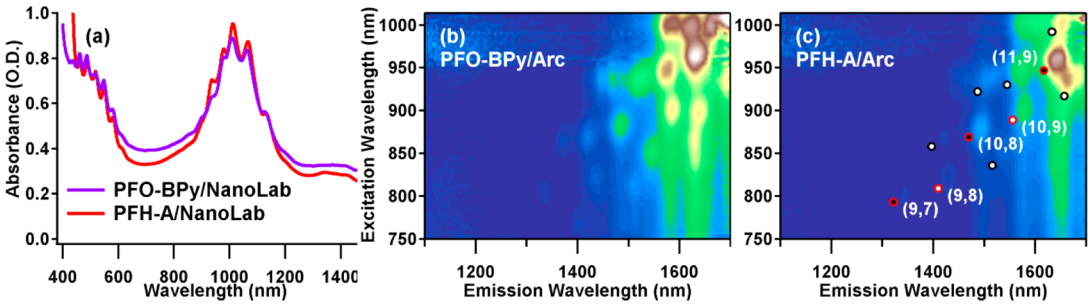

Figure 6. (a) Absorbance spectra of commercial arc-discharge SWCNTs (NanoLab D1L110-J) dispersed by PFO-BPy and PFH-A. Spectra were taken in a 5 mm path length cuvette. (b, c) PLE maps of PFO-BPy/arc-discharge and PFH-A/arc-discharge dispersions, respectively.

efficiency of the polymers around the SWCNT.[11] Copolymers of fluorene and another subunit showed mixed results. While anthracene and bipyridine copolymers (*e.g.*, PFH-A and PFO-BPy) are effective, PFO copolymers with benzothiadiazole and carbazole (PFO-BT and PFO-C) as the alternating subunit do not disperse large-diameter SWCNTs effectively. We also investigated the effect of modifying the copolymer subunit for PFO-BPy to one with a single pyridine and one with a terpyridine group (Supporting Information, Figure S16). Both of these polymers selected a similar range of s-SWCNT chiralities (partially reduced chirality distribution for the monopyridine subunit), but did not offer yields as high as PFO-BPy. Although our empirical results do not allow for a great deal of speculation on *why* certain subunits are particularly effective for dispersing large-diameter SWCNTs, we hope that they serve as a basis for future molecular dynamics studies aimed at exploring both steric and electronic effects. Such modeling efforts, when coupled with the synthetic control over SWCNT starting material demonstrated here, could aid in developing predictive models for polymers designed to select specific SWCNT species across a wide diameter range.

We conclude with a brief discussion of the relevance of these results to commercial processes and devices. For large-scale applications, it may be desired to use commercially available SWCNTs, and it has been suggested that arc-discharge SWCNTs may be less expensive to produce than LV SWCNTs. Figure 6a demonstrates the ability of PFO-BPy and PFH-A to disperse high concentrations of large-diameter s-SWCNTs synthesized *via* arc-discharge (purchased from NanoLab). These arc-discharge SWCNTs provide a larger range of diameters to continue testing and indicate that PFO-BPy and PFH-A are effective regardless of synthesis method.

We further evaluate four key metrics that influence the scalability of our process:

- impurity concentrations: percentage of m-SWCNTs in this case;
- dispersion concentration: mass of SWCNTs per volume of solution;
- yield: percentage of the SWCNTs in the raw material that end up dispersed;
- throughput: amount of desired SWCNT material that can be produced in a given amount of time.

The importance of these metrics is fairly straightforward. Lower m-SWCNT impurity levels lead to devices with better performance and reproducibility, such as PV devices with minimized recombination centers and fewer short-circuited devices and FETs with larger on/off ratios and higher on-currents. Higher dispersion concentrations allow for rapid roll-to-roll deposition of SWCNT films over large areas. Higher yields minimize raw material costs, and higher throughput ensures that SWCNT *ink production* does not constitute a rate-limiting step in a particular fabrication process.

Our earlier analysis demonstrated that m-SWCNT impurity concentrations are kept well below 1% in our polyfluorene LV dispersions. From a TGA/spectroscopy analysis (Supporting Information, Figures S1 and S2), we found that ~1/3 of all s-SWCNTs present in the raw SWCNT material were dispersed by PFO-BPy. Briefly, this analysis revealed that our raw LV SWCNT soot contains ~33% SWCNTs by mass and that the centrifuged dispersion in Figure 1a contains 0.081 ± 0.002 mg/mL, or ~0.81 mg total, of >99.0% s-SWCNTs. Combining this concentration with the SWCNT mass percentage of the raw soot (33%) demonstrates that 33 ± 4% of the semiconducting SWCNTs originally present in the raw SWCNT soot (or ~22% of *all* SWCNTs) are dispersed by PFO-BPy to yield the dark ink demonstrated in Figure 1. Using a conservative estimate of the amount of SWCNT solution we can produce and centrifuge in our lab, *this translates to a lab-scale throughput of several milligrams (up to ~10 mg) of >99% pure s-SWCNTs* ($\langle d \rangle \approx$ *1.3 nm) in under one hour*.

To put this throughput in perspective, it is useful to compare to other separation methods. Although the quantitative yield and throughput are not routinely discussed for DGU and column chromatography studies, one recent study provides a useful benchmark.[38] Feng *et al.* estimated a 27.2% yield of s-SWCNTs for their DGU separation of 1.35 nm SWCNTs, with a total retrieval of approximately 1 mg after DGU, or ~20 μg of SWCNTs per hour when considering the full 48 h

TABLE 1. Table of Key Metrics That Influence Scalability of Our PFO-BPy/LV Dispersions

metric	value	note
electronic purity	>99.0%	s-SWCNTs
impurity level	<1.0%	m-SWCNTs
ink concentration	0.081 ± 0.02 mg/mL	
yield	33 ± 4%	recovered s-SWCNT mass relative to s-SWCNT mass in raw soot
yield	22 ± 3%	recovered s-SWCNT mass relative to mass of all SWCNTs in raw soot
throughput	10 mg/h	retrievable s-SWCNTs with >99.0% purity[a]

[a] Estimated for readily available lab-scale centrifuge capabilities (see Supporting Information).

required to generate the sample. In addition to the significantly lower throughput relative to our polyfluorene dispersions, an important consideration to account for in this comparison is the fact that this DGU study required sonication for 24 h. Several studies have demonstrated that key SWCNT performance metrics for electronics applications, such as conductivity in transparent conducting films or PL quantum yield, are significantly degraded by sonication-induced nanotube shortening, even for sonication times as low as one hour.[22,39] We note that column chromatography should have significantly higher throughput than DGU, but we are unaware of detailed reports on the yield and throughput of this technique for large-diameter SWCNTs, so we cannot comment directly on how our process compares. The metrics addressed in our analysis of the PFO-BPY dispersions are summarized in Table 1.

For certain applications, it may be required to remove or replace excess polymer in solution. For example, films sprayed from these dispersions may need to have reliable nanotube−nanotube connections, and hence minimizing the amount of polymer is needed. Excess polymer can be removed using a solvent extraction technique that involves pelleting out the SWCNTs with additional centrifugation and removing polymer-rich supernatant.[40] Neat solvent can be added to the precipitate to redisperse nanotubes using mild bath sonication. Further polymer removal can be achieved by repeating this process. Another process by which we can remove excess polymer involves filtering solutions through a 0.2 μm Teflon filter, originally developed for removing PFO.[37] Excess polymer washes through, while SWCNTs and bound polymer aggregate into a filter cake, which can be further washed and then redispersed under mild bath sonication. Furthermore, in both of these techniques the polymer-rich supernatant can be reused to disperse new SWCNTs in order to reduce costs, although we have not yet explored the number of cycles for which the polymer selectivity is retained. Recent work has also been reported on exchanging PFO-BT for the photoactive polymer poly(3-hexylthiophene).[41] This technique requires an initial solvent extraction step followed by adding an excess of the desired polymer to displace the fluorene polymer. Another solvent extraction step can then be performed. Polymer exchange could potentially be used to replace PFO-BPy or PFH-A for a number of other polymers relevant to a particular study or device.

CONCLUSIONS

In conclusion, both PFO-BPy and PFH-A demonstrate the ability to select and disperse large-diameter s-SWCNTs with excellent yield, throughput, and purity. PFH-A selectively disperses narrow chirality distributions comprised primarily of near-armchair SWCNTs, with $q = 2$ near-armchair SWCNTs displaying unique solvatochromic shifts. These results indicate that PFH-A has a universal preference for near-armchair SWCNTs over a large diameter range ($\sim$0.8 nm < d < 1.4 nm) and also exerts a unique *family dependence* even within this narrow subset of large chiral angle SWCNTs. The concentrated dispersions enabled by these polymers will allow for semiconducting LV nanotubes to be used in commercially scalable solution-processed devices including FETs and photovoltaics. The bright and narrow PLE spectra permit further studies into individual chiralities whose diameter range can be tuned by careful selection of starting material. Finally, we demonstrate that synthetic control over the SWCNT diameter distribution within a particular synthetic protocol facilitates a better mechanistic understanding of how polyfluorene polymers wrap particular SWCNTs and can also be used to rationally tune chirality distributions for applications.

METHODS

Materials Synthesis. All of the polymers used in this study were purchased from American Dye Source, Inc. and were used without any further purification. Arc-discharge SWCNTs were purchased from NanoLab (D1L110-J) and were also used without further purification.

SWCNTs were prepared in-house at NREL by laser vaporization of a graphite target containing 3% (by weight) each of nickel and cobalt catalysts. Nitrogen was used as the carrier gas for all syntheses, regulated at a flow rate of 150 standard cubic centimeters per minute (sccm) and a constant pressure of 500 Torr. All syntheses employed a Nd:YAG laser, operating in "free run" mode (*i.e.*, not Q-switched) at 1064 nm. The power density for all runs was $\sim$100 W/cm^2. An external furnace surrounding the quartz tube reactor allows for the regulation of synthesis

temperature. The synthesis temperature for most runs was 1125 °C, but was adjusted to several temperatures over the range 800−1175 °C for diameter tuning. For a schematic of the LV synthesis setup, see Figure S9 in the Supporting Information.

SWCNT/Polymer Dispersions. Polymer loadings for Figures 1, 5, and 6 were 2−2.5 mg/mL, while polymer loadings for Figures 2 and 3 were ∼1 mg/mL. All solutions were made in 10 mL of toluene and heated to ∼80 °C for a few minutes to dissolve the polymer. LV SWCNT loading for all samples was approximately 1 mg/mL of raw LV soot. NanoLab arc-discharge loading was higher at ∼4.5 mg/mL because lower loadings led to m-SWCNT impurities (see Supporting Information for a detailed discussion on experimental conditions). Solutions were sonicated with a 1/2 in. probe tip for 30 min at 300 W (Cole-Parmer CPX 750) in a bath of cool (18 °C) flowing water to dissipate heat. Following sonication, solutions were centrifuged at 30000*g* for 5 min using a SW32Ti rotor (Beckman).

The SC solution was 1% SC in D_2O with ∼1 mg/mL raw LV soot. It was sonicated for 30 min with a 1/4 in. probe tip at 225 W (Cole-Parmer CPX 750) in a bath of cool (18 °C) flowing water to dissipate heat and centrifuged for 4 h at 134000*g* using a SW32Ti rotor (Beckman).

To intentionally disperse m-SWCNTs in PFO-BPy (Supporting Information, Figure S6), we decreased the amount of nanotube material used to 1.4 mg in 10 mL of toluene and kept the PFO-BPy concentration above 0.1%. Additionally, we used a purified buckypaper instead of raw soot. The buckypaper was produced by refluxing raw LV SWCNTs in 4 M nitric acid for 16 h and then filtering and washing with water, acetone, and 1 M NaOH to remove impurities generated by the reflux. Following this procedure, the buckypaper was burned rapidly in air at 525 °C to remove amorphous carbon.

Spectroscopy Characterization. All spectroscopic measurements (absorbance, Raman, and PLE) were taken in a 5 mm path length cuvette, except for the SC/LV absorbance, which was taken in a 2 mm path length cuvette to prevent saturation of the detector. Some absorbance spectra in the Supporting Information were taken in 1 mm path length cuvettes and are labeled as such. Absorbance measurements were performed on a Varian Cary 500 spectrophotometer. Raman spectroscopy was performed using a Jobin Yvon 270 M spectrometer with a HeNe excitation laser at 1.96 eV (632.8 nm) in a backscattering configuration. Photoluminescence excitation maps were acquired using a home-built Fourier transform spectrometer as previously described.[42]

For Figure 2, the dispersions were diluted to have the same OD at 935 nm (peak S_{22} OD of the PFO-BPy/LV sample). PL slices were then taken in 5 mm cuvettes to be able to quantitatively compare PL intensity across different samples, as seen in the inset.

Conflict of Interest: The authors declare no competing financial interest.

Supporting Information Available: Quantitative analysis of yield and concentration *via* TGA, full absorbance spectra of PFH-A and PFO-BPY s-SWCNT films and solutions, PL and absorbance spectra of vibronic sidebands, Raman of PFO-BPy prepared to intentionally include m-SWCNTs, Raman of PFH-A, qualitative analysis of s-SWCNT content, schematic of LV synthesis setup, PLE maps for SC, PFO-BPy, and PFH-A dispersions using different LV synthesis temperatures, table of S_{11} and S_{22} peak shifts, absorbance spectra of dispersions using PFO-BPy derivatives with one or three pyridines instead of two, and absorbance spectra of PFO dispersions using different LV synthesis temperatures. This material is available free of charge *via* the Internet at http://pubs.acs.org.

Acknowledgment. This work was supported by the Solar Photochemistry Program of the U.S. Department of Energy, Office of Science, Basic Energy Sciences, Division of Chemical Sciences, Geosciences and Biosciences, under Contract No. DE-AC36-08GO28308 to NREL. We thank Dominick Bindl for helpful discussions.

REFERENCES AND NOTES

1. Jorio, A.; Santos, A.; Ribeiro, H.; Fantini, C.; Souza, M.; Vieira, J.; Furtado, C.; Jiang, J.; Saito, R.; Balzano, L.; *et al*. Quantifying Carbon-Nanotube Species with Resonance Raman Scattering. *Phys. Rev. B* **2005**, *72*, 1–5.
2. Bindl, D. J.; Wu, M.-Y.; Prehn, F. C.; Arnold, M. S. Efficiently Harvesting Excitons from Electronic Type-Controlled Semiconducting Carbon Nanotube Films. *Nano Lett.* **2010**, *11*, 455–460.
3. Holt, J. M.; Ferguson, A. J.; Kopidakis, N.; Larsen, B. A.; Bult, J.; Rumbles, G.; Blackburn, J. L. Prolonging Charge Separation in P3HT-SWNT Composites Using Highly Enriched Semiconducting Nanotubes. *Nano Lett.* **2010**, *10*, 4627–4633.
4. Jain, R. M.; Howden, R.; Tvrdy, K.; Shimizu, S.; Hilmer, A. J.; McNicholas, T. P.; Gleason, K. K.; Strano, M. S. Polymer-Free Near-Infrared Photovoltaics with Single Chirality (6,5) Semiconducting Carbon Nanotube Active Layers. *Adv. Mater.* **2012**, 4436–4439.
5. Chen, Z.; Appenzeller, J.; Knoch, J.; Lin, Y.-m.; Avouris, P. The Role of Metal-Nanotube Contact in the Performance of Carbon Nanotube Field-Effect Transistors. *Nano Lett.* **2005**, *5*, 1497–502.
6. Franklin, A. D.; Luisier, M.; Han, S.-J.; Tulevski, G.; Breslin, C. M.; Gignac, L.; Lundstrom, M. S.; Haensch, W. Sub-10 nm Carbon Nanotube Transistor. *Nano Lett.* **2012**, *12*, 758–762.
7. Izard, N.; Kazaoui, S.; Hata, K.; Okazaki, T.; Saito, T.; Iijima, S.; Minami, N. Semiconductor-Enriched Single Wall Carbon Nanotube Networks Applied to Field Effect Transistors. *Appl. Phys. Lett.* **2008**, *92*, 243112.
8. Lee, S. Y.; Lee, S. W.; Kim, S. M.; Yu, W. J.; Jo, Y. W.; Lee, Y. H. Scalable Complementary Logic Gates with Chemically Doped Semiconducting Carbon Nanotube Transistors. *ACS Nano* **2011**, *5*, 2369–2375.
9. Sangwan, V. K.; Ortiz, R. P.; Alaboson, J. M. P.; Emery, J. D.; Bedzyk, M. J.; Lauhon, L. J.; Marks, T. J.; Hersam, M. C. Fundamental Performance Limits of Carbon Nanotube Thin-Film Transistors Achieved Using Hybrid Molecular Dielectrics. *ACS Nano* **2012**, 7480–7488.
10. Tanaka, T.; Urabe, Y.; Nishide, D.; Kataura, H. Continuous Separation of Metallic and Semiconducting Carbon Nanotubes Using Agarose Gel. *Appl. Phys. Express* **2009**, *2*, 125002.
11. Nish, A.; Hwang, J.-Y.; Doig, J.; Nicholas, R. J. Highly Selective Dispersion of Single-Walled Carbon Nanotubes Using Aromatic Polymers. *Nat. Nanotechnol.* **2007**, *2*, 640–646.
12. Chen, F.; Wang, B.; Chen, Y.; Li, L.-J. Toward the Extraction of Single Species of Single-Walled Carbon Nanotubes Using Fluorene-Based Polymers. *Nano Lett.* **2007**, *7*, 3013–3017.
13. Wang, W. Z.; Li, W. F.; Pan, X. Y.; Li, C. M.; Li, L.-J.; Mu, Y. G.; Rogers, J. A.; Chan-Park, M. B. Degradable Conjugated Polymers: Synthesis and Applications in Enrichment of Semiconducting Single-Walled Carbon Nanotubes. *Adv. Funct. Mater.* **2011**, *21*, 1643–1651.
14. Berton, N.; Lemasson, F.; Tittmann, J.; Stürzl, N.; Hennrich, F.; Kappes, M. M.; Mayor, M. Copolymer-Controlled Diameter-Selective Dispersion of Semiconducting Single-Walled Carbon Nanotubes. *Chem. Mater.* **2011**, *23*, 2237–2249.
15. Tange, M.; Okazaki, T.; Iijima, S. Selective Extraction of Large-Diameter Single-Wall Carbon Nanotubes with Specific Chiral Indices by Poly(9,9-dioctylfluorene-alt-benzothiadiazole). *J. Am. Chem. Soc.* **2011**, *133*, 11908–11911.
16. Yi, X.; Ozawa, H.; Nakagawa, G.; Fujigaya, T.; Nakashima, N.; Asano, T. Single-Walled Carbon Nanotube Thin Film Transistor Fabricated Using Solution Prepared with 9,9-Dioctyfluorenyl-2,7-diyl−Bipyridine Copolymer. *Jpn. J. Appl. Phys.* **2011**, *50*, 070207.
17. Zhou, X.; Park, J.-Y.; Huang, S.; Liu, J.; McEuen, P. Band Structure, Phonon Scattering, and the Performance Limit of Single-Walled Carbon Nanotube Transistors. *Phys. Rev. Lett.* **2005**, *95*, 1–4.
18. Peet, J.; Kim, J. Y.; Coates, N. E.; Ma, W. L.; Moses, D.; Heeger, A. J.; Bazan, G. C. Efficiency Enhancement in Low-Bandgap

Polymer Solar Cells by Processing with Alkane Dithiols. *Nat. Mater.* **2007**, *6*, 497–500.
19. Coffey, D. C.; Larson, B. W.; Hains, A. W.; Whitaker, J. B.; Kopidakis, N.; Boltalina, O. V.; Strauss, S. H.; Rumbles, G. An Optimal Driving Force for Converting Excitons into Free Carriers in Excitonic Solar Cells. *J. Phys. Chem. C* **2012**, *116*, 8916–8923.
20. Wang, S.; Khafizov, M.; Tu, X.; Zheng, M.; Krauss, T. D. Multiple Exciton Generation in Single-Walled Carbon Nanotubes. *Nano Lett.* **2010**, *10*, 2381–2386.
21. Hasan, T.; Sun, Z.; Wang, F.; Bonaccorso, F.; Tan, P. H.; Rozhin, A. G.; Ferrari, A. C. Nanotube-Polymer Composites for Ultrafast Photonics. *Adv. Mater.* **2009**, *21*, 3874–3899.
22. Tenent, R. C.; Barnes, T. M.; Bergeson, J. D.; Ferguson, A. J.; To, B.; Gedvilas, L. M.; Heben, M. J.; Blackburn, J. L. Ultrasmooth, Large-Area, High-Uniformity, Conductive Transparent Single-Walled-Carbon-Nanotube Films for Photovoltaics Produced by Ultrasonic Spraying. *Adv. Mater.* **2009**, *21*, 3210–3216.
23. Lebedkin, S.; Hennrich, F.; Kiowski, O.; Kappes, M. M. Photophysics of Carbon Nanotubes in Organic Polymer-Toluene Dispersions: Emission and Excitation Satellites and Relaxation Pathways. *Phys. Rev. B* **2008**, *77*, 1–8.
24. Arnold, M. S.; Green, A. A.; Hulvat, J. F.; Stupp, S. I.; Hersam, M. C. Sorting Carbon Nanotubes by Electronic Structure Using Density Differentiation. *Nat. Nanotechnol.* **2006**, *1*, 60–65.
25. Blackburn, J. L.; Holt, J. M.; Irurzun, V. M.; Resasco, D. E.; Rumbles, G. Confirmation of K-Momentum Dark Exciton Vibronic Sidebands Using ^{13}C-Labeled, Highly Enriched (6,5) Single-Walled Carbon Nanotubes. *Nano Lett.* **2012**, *12*, 1398–1403.
26. Dresselhaus, M.; Dresselhaus, G.; Saito, R.; Jorio, A. Raman Spectroscopy of Carbon Nanotubes. *Phys. Rep.* **2005**, *409*, 47–99.
27. Polymer:SWCNT concentrations can be intentionally tuned to reduce the selectivity of PFO-BPy for s-SWCNTs. In this case, we are able to see signatures such as the G band that match those seen in the SC/LV sample (see Supporting Information), demonstrating that the characteristic m-SWCNTs appear identical in both samples.
28. Engel, M.; Small, J. P.; Steiner, M.; Freitag, M.; Green, A. A.; Hersam, M. C.; Avouris, P. Thin Film Nanotube Transistors Based on Self-Assembled, Aligned, Semiconducting Carbon Nanotube Arrays. *ACS Nano* **2008**, *2*, 2445–2452.
29. Moshammer, K.; Hennrich, F.; Kappes, M. M. Selective Suspension in Aqueous Sodium Dodecyl Sulfate According to Electronic Structure Type Allows Simple Separation of Metallic from Semiconducting Single-Walled Carbon Nanotubes. *Nano Res.* **2009**, *2*, 599–606.
30. Tanaka, T.; Jin, H.; Miyata, Y.; Kataura, H. High-Yield Separation of Metallic and Semiconducting Single-Wall Carbon Nanotubes by Agarose Gel Electrophoresis. *Appl. Phys. Express* **2008**, *1*, 114001.
31. Blackburn, J. L.; Barnes, T. M.; Beard, M. C.; Kim, Y.-H.; Tenent, R. C.; McDonald, T. J.; To, B.; Coutts, T. J.; Heben, M. J. Transparent Conductive Single-Walled Carbon Nanotube Networks with Precisely Tunable Ratios of Semiconducting and Metallic Nanotubes. *ACS Nano* **2008**, *2*, 1266–1274.
32. Weisman, R. B.; Bachilo, S. M. Dependence of Optical Transition Energies on Structure for Single-Walled Carbon Nanotubes in Aqueous Suspension: An Empirical Kataura Plot. *Nano Lett.* **2003**, *3*, 1235–1238.
33. Larsen, B. A.; Deria, P.; Holt, J. M.; Stanton, I. N.; Heben, M. J.; Therien, M. J.; Blackburn, J. L. Effect of Solvent Polarity and Electrophilicity on Quantum Yields and Solvatochromic Shifts of Single-Walled Carbon Nanotube Photoluminescence. *J. Am. Chem. Soc.* **2012**, *134*, 12485–12491.
34. Silvera-Batista, C. A.; Wang, R. K.; Weinberg, P.; Ziegler, K. J. Solvatochromic Shifts of Single-Walled Carbon Nanotubes in Nonpolar Microenvironments. *Phys. Chem. Chem. Phys.* **2010**, *12*, 6990–6998.
35. Fagan, J. A.; Huh, J. Y.; Simpson, J. R.; Blackburn, J. L.; Holt, J. M.; Larsen, B. A.; Walker, A. R. H. Separation of Empty and Water-Filled Single-Wall Carbon Nanotubes. *ACS Nano* **2011**, *5*, 3943–3953.
36. Kataura, H.; Kumazawa, Y.; Maniwa, Y.; Ohtsuka, Y.; Sen, R.; Suzuki, S.; Achiba, Y. Diameter Control of Single-Walled Carbon Nanotubes. *Carbon* **2000**, *38*, 1691–1697.
37. Gao, J.; Loi, M. A.; de Carvalho, E. J. F.; Dos Santos, M. C. Selective Wrapping and Supramolecular Structures of Polyfluorene-Carbon Nanotube Hybrids. *ACS Nano* **2011**, *5*, 3993–3999.
38. Feng, Y.; Miyata, Y.; Matsuishi, K.; Kataura, H. High-Efficiency Separation of Single-Wall Carbon Nanotubes by Self-Generated Density Gradient Ultracentrifugation. *J. Phys. Chem. C* **2011**, *115*, 1752–1756.
39. Mouri, S.; Miyauchi, Y.; Matsuda, K. Dispersion-Process Effects on the Photoluminescence Quantum Yields of Single-Walled Carbon Nanotubes Dispersed Using Aromatic Polymers. *J. Phys. Chem. C* **2012**, *116*, 10282–10286.
40. Schuettfort, T.; Snaith, H. J.; Nish, A.; Nicholas, R. J. Synthesis and Spectroscopic Characterization of Solution Processable Highly Ordered Polythiophene–Carbon Nanotube Nanohybrid Structures. *Nanotechnology* **2010**, *21*, 025201.
41. Stranks, S. D.; Yong, C.-K.; Alexander-Webber, J. A.; Weisspfennig, C.; Johnston, M. B.; Herz, L. M.; Nicholas, R. J. Nanoengineering Coaxial Carbon Nanotube–Dual-Polymer Heterostructures. *ACS Nano* **2012**, *6*, 6058–6066.
42. McDonald, T. J.; Jones, M.; Engtrakul, C.; Ellingson, R. J.; Rumbles, G.; Heben, M. J. Near-Infrared Fourier Transform Photoluminescence Spectrometer with Tunable Excitation for the Study of Single-Walled Carbon Nanotubes. *Rev. Sci. Instrum.* **2006**, *77*, 053104.